Phonon-assisted broadening in Bernal boron nitride: A comparison between indirect and direct excitons

A. Rousseau [1], P. Valvin [1], L. Xue [2], J. Li [2], J. H. Edgar [2], B. Gil [1], and G. Cassabois [1,*]

[1]*Laboratoire Charles Coulomb, UMR 5221, CNRS-Université de Montpellier, 34095 Montpellier, France*
[2]*Tim Taylor Department of Chemical Engineering, Kansas State University, Manhattan, Kansas 66506, USA*

We study the deep-ultraviolet emission in Bernal boron nitride as a function of temperature. The quasidegeneracy of indirect and direct excitons in Bernal boron nitride leads to their simultaneous recombination, allowing a comparison of phonon-assisted broadening in the two cases. Temperature-dependent measurements reveal that below 200 K, the efficiency of phonon-assisted broadening is one order of magnitude lower for the direct transition at 6.035 eV than for the phonon replicas of the indirect exciton. This striking effect results from the inhibition of quasielastic acoustic phonon scattering in the strong-coupling regime of the light-matter interaction, where the density of final states is reduced by the curvature of the polaritonic dispersion.

I. INTRODUCTION

Hexagonal boron nitride (hBN) is a wide-band-gap semiconductor which differs from other nitrides because of its sp^2 hybridized bonds forming honeycomb atomic planes weakly stacked through the van der Waals interaction [1]. Since the first synthesis of large hBN single crystals by Watanabe *et al.* in 2004 [2], hBN has become a pivotal material in a wide variety of applications such as photonics, optronics, neutronics, and twistronics [3,4]. hBN corresponds to the so-called *AA'* stacking of atomic planes, where boron and nitrogen atoms alternate along the *c* axis [5]. This is the most common sp^2-bonded boron nitride polytype. Other polytypes have different stacking sequences of the basal plane: Bernal boron nitride (bBN) with an *AB* stacking, rhombohedral boron nitride (rBN) with an *ABC* stacking, and also turbostratic boron nitride (tBN), which differs from the previous two by the existence of some translational and rotational disorder in the vertical stacking [6–8].

The bBN is isostructural to graphite and, like hBN, it has a band gap in the range of ∼6 eV [9–11]. Still, the different stackings lead to subtle modifications of the electronic and optical properties [10–14]. On the one hand, the independent-particle dispersions of hBN and bBN both exhibit a conduction band minimum at the *M* point, and the valence band maximum around the *K* point. This results in free electron-hole pairs with a minimum of their energy dispersion at the *T* point of the first Brillouin zone in both hBN and bBN. Direct band-to-band transitions occur at higher energies, but with a relative blueshift that depends on the stacking. In hBN, the direct single-particle gap is ∼0.5 eV higher in energy than the fundamental indirect gap, while this value decreases to less than 0.2 eV in bBN [12]. This effect stems from the flatter dispersion of the conduction band for the *AB* stacking [12–14]. The attractive electron-hole interaction further modifies the picture, with different binding energies of direct and indirect excitons [12–14]. In hBN, the direct exciton dX_h lies at 6.125 eV [15], i.e., an energy 0.17 eV higher than the fundamental indirect exciton iX_h at 5.955 eV [9]. On the contrary, in bBN, the direct exciton dX_b is quasidegenerate with the indirect one iX_b, in which calculations have predicted a marginally direct optical gap [12] while recent experiments have shown it to be marginally indirect [11]. The quasidegeneracy of dX_b and iX_b is the signature of an unusually flat in-plane dispersion of the excitonic states in bBN that allows their simultaneous observation in luminescence experiments [11].

In this paper, we study the deep-ultraviolet photoluminescence (PL) in bBN as a function of temperature. The thermal broadening is extracted for both the direct emission line at ∼6.035 eV and the phonon replicas of iX_b below 6 eV. We observe drastically different broadening behaviors. In the first case, for the direct emission line related to dX_b, the thermal broadening is linear with the phonon occupation factor $n(T)$. In the second case, for the phonon replicas of iX_b, the thermal broadening scales like the square root of $n(T)$. Moreover, below 200 K, the efficiency of phonon-assisted broadening is one order of magnitude lower for the direct transition at ∼6.035 eV than for the phonon replicas of iX_b. We interpret the different phenomenologies of phonon-assisted dephasing as a result of the strong-coupling regime of the light-matter interaction for dX_b, where the density of final states is reduced by the curvature of the polaritonic dispersion.

II. EXPERIMENTAL RESULTS

Our measurements are performed in the experimental conditions of Ref. [11]. The hBN and bBN crystals are extracted from a polytypic sp^2-bonded carbon-doped BN crystal precipitated from a metal solution, as described in Refs. [10,16]. Such a polycrystal contains novel shallow and
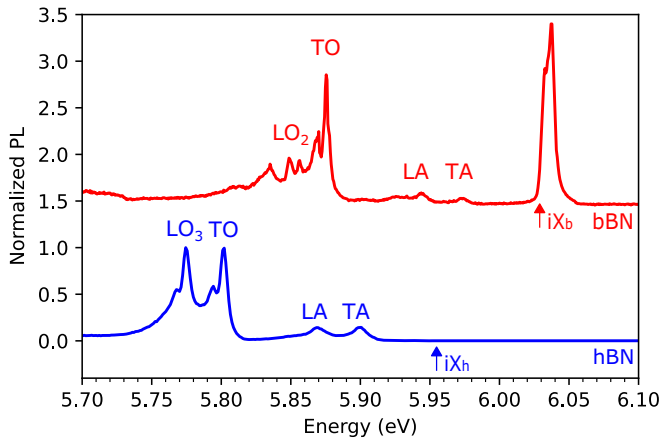
*guillaume.cassabois@umontpellier.fr

FIG. 1. PL spectra at 6 K recorded for bBN (top, red line) and hBN (bottom, blue line) crystals. PL excitation energy = 6.39 eV. The bBN spectrum is vertically shifted for clarity.
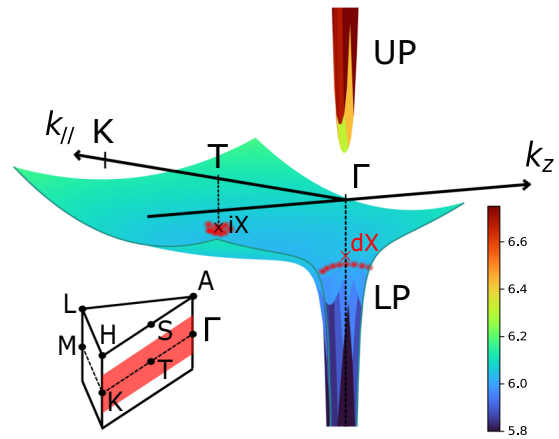

FIG. 2. Schematic representation of the dispersion of the upper (UP) and lower (LP) polaritons due to level anticrossing between excitons and photons in bBN, in the half space $\{k_\parallel > 0\}$. The red dots indicate the accumulated populations (i) at the minimum of the excitonic dispersion (iX_b) around the T point of the Brillouin zone in the middle of the ΓK line (at an energy of 6.029 eV), and (ii) at the relaxation bottleneck on the lower-polariton branch, close to the zone center Γ (at an energy $\sim$6.035 eV, slightly below the bare dX_b energy). Inset: irreducible part of the first Brillouin zone, where the red area indicates the landscape of the dispersion plot.

deep levels emitting at $\sim$5.45 and $\sim$4.14 eV, respectively [16]. The extracted hBN and bBN crystals are presently studied in a scanning confocal cryomicroscope operating in the deep-ultraviolet range [17,18], which was a pivotal tool for identifying bBN crystals [11]. The PL signal is collected along the c axis of the crystals.

A. Quasidegeneracy of direct and indirect excitons in bBN

The PL spectra of hBN and bBN are displayed in Fig. 1 in the spectral range between 5.7 and 6.1 eV. As explained in our recent publication [11], hBN and bBN have different emission spectra in the deep-ultraviolet range. In the case of hBN (bottom blue line, Fig. 1), the intrinsic emission only results from the phonon-assisted recombination of iX_h, which is located at the T point of the first Brillouin zone at an energy of 5.955 eV [9,19–21]. For an electromagnetic field propagating along the c axis, four different phonon modes are symmetry allowed in the phonon-assisted processes, namely, LO_3, TO, LA, and TA, as noted on the blue spectrum of Fig. 1. Moreover, there is a fine structure of the phonon replicas coming from higher-order processes involving overtones of the interlayer shear mode [22]. There is no signature of the direct exciton dX_h in the PL spectrum of hBN.

The PL spectrum of bBN (top red line, Fig. 1) is related to both the direct (dX_b) and indirect (iX_b) excitons. The series of lines between 5.84 and 6 eV stems from the phonon-assisted recombination of iX_b, which sits at an energy of 6.029 eV (as indicated in Fig. 1). The bBN phonon replicas are blueshifted by $\sim$74 meV with respect to the ones of hBN: the LA and TA phonon replicas of bBN occur at $\sim$5.94 and $\sim$5.97 eV, respectively, and the LO_2 and TO replicas at $\sim$5.85 and $\sim$5.87 eV [11]. iX_b appears almost resonant with the $\sim$6.035 eV line. This line and its phonon replica at $\sim$5.835 eV are linked to the direct exciton dX_b [10,11]. Because of the direct nature of dX_b, the strong-coupling regime of the light-matter interaction notably modifies the excitonic dispersion so that the $\sim$6.035 eV line only gives a lower bound for the dX_b energy, as detailed in the next part. Still, the direct and indirect excitons are quasidegenerate in bBN, a peculiarity explaining their simultaneous emission.

B. Strong light-matter interaction

Due to the three-dimensional (3D) translational invariance of the system, direct excitons in bulk crystals strongly couple to light [23–25]. The new eigenstates are mixed exciton-photon states, the so-called exciton polaritons, with the lower polariton (LP) and upper polariton (UP) branches (Fig. 2).

Figure 2 is a schematic representation of their energy dispersions in bBN. Here we plot the energy levels in a two-dimensional momentum space defined by the in-plane and out-of-plane wave vectors $k_\parallel$ and k_z, respectively (k_z being parallel to the c axis), focusing on the ΓK line of the first Brillouin zone. The bare excitonic states are weakly dispersed along the c axis because of the weak van der Waals interaction between adjacent layers. This is also the case for the in-plane dispersion, along the ΓK line in bBN, as discussed above and calculated by Sponza *et al.* [12]. The direct exciton dX_b is located at $\mathbf{k} \sim 0$, while the indirect one iX_b is nested at the T point, approximately in the middle of the ΓK line [12], as shown in Fig. 2.

Each excitonic state of a given $\mathbf{k}$ interacts with a photon of the same wave vector because of the momentum conservation rule arising from the 3D translational invariance of the system. The polaritonic dispersions significantly deviate from the bare excitonic one around the light cone, i.e., for the direct state dX_b. The UP branch is split from the bare exciton state by the so-called longitudinal-transverse splitting Δ_{LT} [25]. This splitting takes giant values in hBN ($\Delta_{LT} = 420$ meV) because of the existence of electronic flat bands in the independent-particle band structure [15]. We anticipate an ultralarge value also in bBN because of the similarity of the band structures of hBN and bBN. On the high-energy side of the reststrahlen band, with width Δ_{LT}, the polaritons have a photonlike character (UP in Fig. 2). On the low-energy side,

for large wave vectors far from the light cone, the LP branch closely follows the excitonic dispersion, with an excitonlike character of the exciton polaritons. On the contrary, when approaching the anticrossing, the photonic component of the LP states increases, with a more and more pronounced bending of the LP dispersion (Fig. 2). Such a curvature of the LP dispersion results in the well-documented bottleneck effect for carrier relaxation in direct bulk semiconductors [23–25]. We will show below that it also plays a key role in the interpretation of the thermal broadening in bBN. Close to the light cone, the LP branch finally closely follows the photonic dispersion.

Because exciton polaritons are the eigenstates of bulk semiconductors coupled to light, there is no radiative decay of a direct exciton in an ideal crystal. In other words, there is no luminescence from a direct exciton in a perfect crystal. The luminescence from a bulk semiconductor comes from the polariton recombination, which results from the complex interplay between propagation, damping, and thermalization processes [25]. Thermalization is very efficient down to the knee of the LP branch, which creates the relaxation bottleneck where polaritons accumulate (as indicated by the red dots around Γ in Fig. 2). Therefore, the luminescence peak is not at an energy corresponding to the direct exciton, but it is slightly below. This is the reason why the $\sim$6.035 eV emission line provides a lower bound for the dX_b energy ($E_{dX_b} > 6.035$ eV).

The overall picture for the population relaxation dynamics in bBN is thus the following: the laser excitation at $\sim$6.39 eV leads to the creation of electron-hole pair states in the absorption continuum; then the photogenerated carriers relax either towards iX_b at the minimum of the excitonic dispersion around the T point of the Brillouin zone along the ΓK line (red dots around T, Fig. 2) or along the lower-polariton branch where they accumulate at the relaxation bottleneck around $\sim$6.035 eV, slightly below the dX_b energy (red dots around Γ, Fig. 2). Given the quasidegeneracy of the involved states, there is no efficient relaxation channel between them, leading to simultaneous direct and indirect transitions of comparable efficiency in bBN.

C. Phonon-assisted broadening

The strong-coupling regime of the light-matter interaction further impacts the coherence relaxation dynamics in bBN. By temperature-dependent PL measurements, we demonstrate that the phonon-assisted broadening has a radically different efficiency for iX_b and for the polariton formed from dX_b.

The PL spectra of bBN are recorded from 6 to 250 K in the same conditions as in Fig. 1. Figure 3 is a zoom of the direct emission line at $\sim$6.035 eV for different temperatures. The phonon replicas of iX_b below 6 eV display a phenomenology similar to the ones of iX_h in hBN [26]. In Fig. 3, we observe a thermal broadening of the PL line above 50 K, together with a redshift down to $\sim$6.02 eV at 210 K. The PL intensity decreases by a factor of 20 between 10 and 250 K. Interestingly, we note the existence of a weaker peak at higher energy ($\sim$14 meV above), showing the same redshift as a function of temperature as the intense $\sim$6.035 eV line (see the parallel dotted lines in Fig. 3).
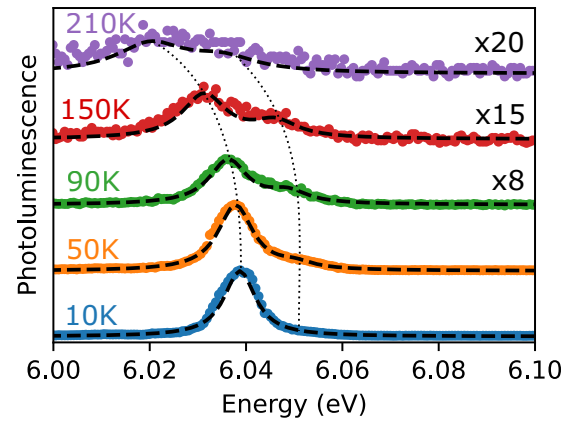

FIG. 3. PL spectra in bBN above 6 eV as a function of temperature: data (symbols) and fit following the bimodal distribution of Eq. (A1) (dashed lines). The spectra are vertically shifted for clarity. The dotted lines are guides for the eyes.

In order to extract the thermal broadening, the PL spectra are fitted with the convolution of a line of width Γ, accounting for homogeneous broadening, with a distribution function $\mathcal{F}$. For the indirect exciton iX_b, the homogeneous linewidth is denoted Γ_i, and the distribution function $\mathcal{F}_i$ is the series of phonon replicas of the LO_2/TO doublet with a detuning given by the energy of the corresponding phonon modes involved in the phonon-assisted process, as detailed in Refs. [22,26] for hBN. For the direct emission line at $\sim$6.035 eV, the linewidth is denoted Γ_d, and $\mathcal{F}_d$ is an *ad hoc* bimodal function phenomenologically describing the thermalized population of exciton polaritons at the bottleneck of the lower-polariton branch, as explained in the Appendix. Namely, we use two Lorentzian lines of the same width Γ_d to fit the PL spectra above 6 eV.

Figure 4 summarizes the results of our data analysis for both Γ_i and Γ_d. In this figure are displayed the variations of the broadening with respect to 10 K [$\Delta\Gamma(T) = \Gamma_\alpha(T) - \Gamma_\alpha(10\,\mathrm{K})$, where $\alpha = i$ or d]. The results are drastically different in the two cases. For the indirect exciton iX_b (orange squares in Fig. 4), the phonon-assisted broadening reaches values as high as $\sim$20 meV at 100 K before a slower increase up to 50 meV at higher temperatures. In this case, the thermal broadening shows the same unusual curvature as for the indirect exciton iX_h in hBN (dashed line in Fig. 4, adapted from Ref. [26]). On the contrary, for the direct emission at $\sim$6.035 eV related to dX_b (blue circles in Fig. 4), phonon dephasing is much less efficient than for iX_b, by approximately one order of magnitude below 200 K, before an exponential increase after 200 K. In that case, we recover the standard phenomenology of semiconductor physics [27].

The unusual curvature of the temperature variations of Γ_i stems from the so-called slow modulation limit of the phonon-assisted broadening predicted by Toyozawa in his seminal paper [28], and first observed in hBN [26]. In the slow modulation limit, each contribution to the phonon-assisted broadening scales like the square root of the phonon occupation number, so that the total phonon dephasing is written
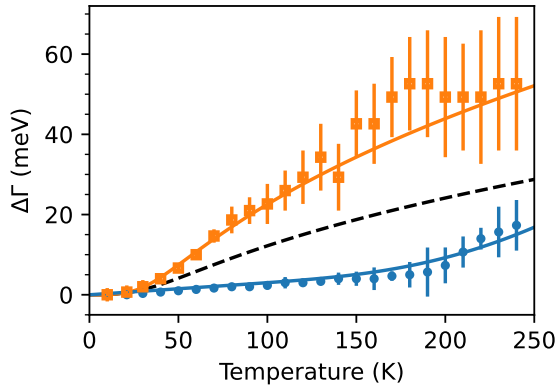
FIG. 4. Thermal broadening of the indirect exciton iX_b (orange squares), and of the lower exciton-polariton related to dX_b (blue circles) in bBN. $\Delta\Gamma(T) = \Gamma_\alpha(T) - \Gamma_\alpha(10\,\text{K})$ where $\alpha = i$ for the broadening of the indirect exciton iX_b, or $\alpha = d$ for the broadening of the direct emission at ~ 6.035 eV. The dashed line is the thermal broadening of the indirect exciton iX_h in hBN, adapted from Ref. [26]. The orange solid line is a fit with Eq. (1) with the fitting parameters $E_A = 4$ meV, $E_O = 15$ meV, $S_A = 4.5$ meV, and $S_O = 200$ meV. The blue solid line is a fit with Eq. (4) with the fitting parameters $a = 0.03$ meV K^{-1}, $b = 600$ meV, and $\Lambda = 90$ meV.

as [26]

$$\Gamma_i(T) - \Gamma_i(0) = \sqrt{\Delta_A^2 + \Delta_O^2} - \sqrt{S_A E_A}, \tag{1}$$

where Δ_A and Δ_O are the contributions of acoustic and optical phonons, respectively, given by [28]

$$\Delta_A^2 = S_A E_A \coth\left(\frac{E_A}{2k_B T}\right), \tag{2}$$

$$\Delta_O^2 = S_O E_O \frac{1}{e^{\frac{E_O}{k_B T}} - 1}, \tag{3}$$

where E_A and E_O represent the mean energy of the acoustic and optical phonons involved in the dephasing processes, respectively, S_A and S_O are the corresponding coupling strengths, and k_B is the Boltzmann constant. The term $\sqrt{S_A E_A}$ in Eq. (1) corresponds to the nonzero limit of Δ_A at $T = 0$, which has to be subtracted to compare with the experimental thermal broadening $\Delta\Gamma$. A fair agreement with our data is obtained by taking $E_A = 4$ meV, $E_O = 15$ meV, $S_A = 4.5$ meV, and $S_O = 200$ meV (orange line on Fig. 4). The phonon dephasing is in the slow modulation limit in bBN as in hBN because of the weakly dispersed excitonic bands in these two BN polytypes, fulfilling Toyozawa's criterion of "flat bands" [28]. Remarkably, an enhancement by a factor ~ 2 is observed in bBN in comparison to the thermal broadening of the indirect exciton iX_h in hBN (black dashed line on Fig. 4). We interpret this effect as a result of the weak excitonic dispersion, not only along the c axis, but also in the plane of the layers in bBN, as discussed above (Fig. 2), and witnessed by the quasidegeneracy of iX_b and dX_b.

The thermal broadening of the direct emission at ~ 6.035 eV related to dX_b (blue circles in Fig. 4) cannot

be explained by the slow modulation of phonon dephasing, but, on the contrary, by the fast modulation limit for which the linewidth increases linearly with the phonon occupation number $n(T)$. Such a difference comes from the motional narrowing regime of the exciton-phonon interaction that is quasiuniversal in semiconductor physics [26–28], leading to the well-known phonon dephasing,

$$\Gamma_d(T) - \Gamma_d(0) = \Xi_A + \Xi_O, \tag{4}$$

where Ξ_A and Ξ_O are the contributions of acoustic and optical phonons, respectively, given by [27]

$$\Xi_A = aT, \tag{5}$$

$$\Xi_O = b\frac{1}{e^{\frac{\Lambda}{k_B T}} - 1}, \tag{6}$$

where a and b characterize the coupling to acoustic and optical phonons, respectively, and Λ is the typical optical phonon energy. An excellent agreement with our data is obtained with $a = 0.03$ meV K^{-1}, $b = 600$ meV, and $\Lambda = 90$ meV. The dramatic modification of the thermal broadening with respect to the indirect exciton iX_b originates from the strong-coupling regime of the light-matter interaction in the case of dX_b. Because one has to consider the density of polaritonic states, and not the density of excitonic states, in the calculations of phonon dephasing within the Fermi's golden rule [27], the curvature of the polaritonic dispersions leads to a reduction of the density of final states. This is particularly important for polaritons at the relaxation bottleneck (Fig. 2) that are quasielastically scattered at high **k** by acoustic phonons [27]. Here, the reduced density of final states modifies the phonon dephasing efficiency both qualitatively and quantitatively. First, there is a transition from the slow modulation limit [Eq. (1)] to the fast one [Eq. (4)], with different curvatures of the broadening as a function of temperature (Fig. 4), because Toyozawa's criterion of "flat bands" is no longer fulfilled. Second, there is an overall decrease of the phonon dephasing efficiency, by approximately one order of magnitude below 200 K (Fig. 4), when quasielastic acoustic phonon scattering dominates.

Although the impact of the polariton formation on the phonon dephasing was pointed out earlier and calculated in Ref. [27], we are not aware of any demonstration for exciton polaritons, even though an analogous and moderate effect was reported for cavity polaritons in two-dimensional systems [29]. The bBN appears as a model system for demonstrating the influence of the reduced density of polaritonic states in quasielastic acoustic phonon dephasing since the quasidegeneracy of iX_b and dX_b allows a direct comparison of the corresponding thermal broadening below 200 K, as seen in Fig. 4.

Above 200 K, the broadening processes assisted by optical phonons become more and more important. Such scattering mechanisms are no longer quasielastic so that they involve other final states than the polaritons of the lower branch. As a consequence, the thermal broadening starts to converge to similar values above 200 K (Fig. 4). Although the signal-to-noise ratio was too small to accurately estimate the homogeneous linewidth above 250 K up to room temperature, we note that the thermal broadening of iX_b and dX_b already

differs by only a factor ~ 3 around 250 K, while it was by one order of magnitude at ~ 200 K.

III. CONCLUSION

We have studied the thermal broadening in bBN crystals by means of temperature-dependent PL measurements in the deep-ultraviolet range. The quasidegeneracy of the indirect and direct excitons in bBN allows a unique comparison of the phonon dephasing efficiency in the two cases. For the indirect exciton iX_b, the phonon-assisted broadening is qualitatively identical to the indirect exciton in hBN, i.e., in the slow modulation of phonon dephasing, but with an enhancement by a factor ~ 2 due to the weak in-plane excitonic dispersion in bBN. For the direct emission at ~ 6.035 eV related to dX_b, the thermal broadening switches to the standard fast modulation limit, with a reduction by approximately one order of magnitude of the phonon dephasing efficiency below 200 K. This striking effect results from the inhibition of quasielastic acoustic phonon scattering due to the reduced density of final states along the polaritonic dispersion. The thermal broadening in bBN provides a textbook example for the diversity of phonon dephasing in excitons, and the influence of the strong-coupling regime of the light-matter interaction in the case of direct excitons. Our work also illustrates the wealth of original effects to be explored in the recently identified Bernal polytype of boron nitride.

APPENDIX: LINESHAPE FITTING OF THE DIRECT EMISSION AT ~ 6.035 eV

A fair agreement with the experimental data at ~ 6.035 eV is reached by taking, for the PL signal intensity $I(E)$, the sum of two Lorentzian functions of the same width Γ and of amplitudes $\mathcal{A}_j$:

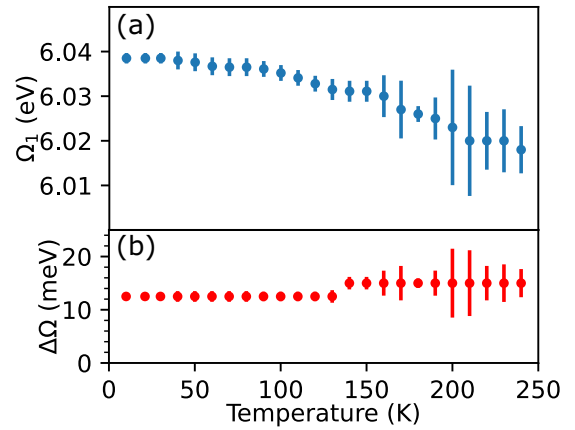$$I(E) = \sum_{j=1}^{2} \mathcal{A}_j L_j(E), \qquad (A1)$$

FIG. 5. Temperature variations of the (a) central energy Ω_1 and (b) energy splitting $\Omega_2 - \Omega_1$.

where $L_j(E)$ is a normalized Lorentzian function,

$$L_j(E) = \frac{1}{\pi} \frac{\frac{\Gamma}{2}}{(E - \Omega_j)^2 + \left(\frac{\Gamma}{2}\right)^2}, \qquad (A2)$$

with Ω_j the central energy and $\Omega_2 > \Omega_1$.

$\{\Gamma, \mathcal{A}_j, \Omega_j\}$ are free parameters, which are adjusted for each temperature to reproduce our experimental data (Fig. 4). The temperature variations of the energy Ω_1 and of the energy splitting $\Omega_2 - \Omega_1$ are displayed in Figs. 5(a) and 5(b), respectively. The thermal redshift of $L_1(E)$ centered at Ω_1 comes from the temperature dependence of the bBN band gap, with a decrease of ~ 20 meV from 10 to 250 K [Fig. 5(a)], similar to the one observed in hBN [19]. The energy splitting $\Omega_2 - \Omega_1$ of about ~ 14 meV is approximately constant with temperature, within our experimental error [Fig. 5(b)]. The discontinuity of the energy splitting $\Omega_2 - \Omega_1$ at ~ 130 K is attributed to a spatial drift of the sample when changing the temperature.

Since the high-energy component of the PL spectrum centered at Ω_2 is more and more intense when raising the temperature (Fig. 5), the ratio $\mathcal{A}_2/\mathcal{A}_1$ increases with temperature, suggesting a thermal activation. We find that $\mathcal{A}_2/\mathcal{A}_1$ follows a Boltzmann law $\exp(-E_0/k_B T)$, with E_0 of the order of the energy splitting, $\Omega_2 - \Omega_1$. More precisely, the best fit to the experimental data is obtained by taking, for E_0, the energy splitting $\Omega_2 - \Omega_1$, but with a small correction of -2 meV.

From this quantitative interpretation of the direct emission at ~ 6.035 eV, we thus conclude that the bimodal PL lineshape observed in Fig. 5 originates from a two-component distribution of thermalized exciton polaritons at the bottleneck of the lower-polariton branch. At this stage, we have no clear interpretation for the origin of these two peaks, which will require further investigation beyond the scope of this work.

[1] W. H. Balmain, J. Prakt. Chem. **27**, 422 (1842).

[2] K. Watanabe, T. Taniguchi, and H. Kanda, Nat. Mater. **3**, 404 (2004).

[3] J. Caldwell, I. Aharonovich, G. Cassabois, J. H. Edgar, B. Gil, and D. N. Basov, Nat. Rev. Mater. **4**, 552 (2019).

[4] B. Gil, G. Cassabois, R. Cuscó, G. Fugallo and L. Artús, Nanophotonics **9**, 3483 (2020).

[5] R. S. Pease, Acta Cryst. **5**, 356 (1952).

[6] M. I. Petrescu and M. G. Balint, U.P.B. Sci. Bulletin, Series B **69**, 35 (2007).

[7] G. Constantinescu, A. Kuc, and T. Heine, Phys. Rev. Lett. **111**, 036104 (2013).

[8] M. Moret, A. Rousseau, P. Valvin, S. Sharma, L. Souqui, H. Pedersen, H. Högberg, G. Cassabois, J. Li, J. H. Edgar, and B. Gil, Appl. Phys. Lett. **119**, 262102 (2021).

[9] G. Cassabois, P. Valvin, and B. Gil, Nat. Photon. **10**, 262 (2016).

[10] A. Rousseau, M. Moret, P. Valvin, W. Desrat, J. Li, E. Janzen, L. Xue, J. H. Edgar, G. Cassabois, and B. Gil, Phys. Rev. Materials **5**, 064602 (2021).

[11] A. Rousseau, P. Valvin, W. Desrat, L. Xue, J. Li, J. H. Edgar, G. Cassabois, and B. Gil, ACS Nano **16**, 2756 (2022).

[12] L. Sponza, H. Amara, C. Attaccalite, S. Latil, T. Galvani, F. Paleari, L. Wirtz, and F. Ducastelle, Phys. Rev. B **98**, 125206 (2018).

[13] K. A. Mengle and E. Kioupakis, APL Mater. **7**, 021106 (2019).

[14] S. M. Gilbert, T. Pham, M. Dogan, S. Oh, B. Shevitski, G. Schumm, S. Liu, P. Ercius, S. Aloni, M. L. Cohen, and A. Zettl, 2D Mater. **6**, 021006 (2019).

[15] C. Elias, G. Fugallo, P. Valvin, C. L'Henoret, J. Li, J. H. Edgar, F. Sottile, M. Lazzeri, A. Ouerghi, B. Gil, and G. Cassabois, Phys. Rev. Lett. **127**, 137401 (2021).

[16] T. Pelini, C. Elias, R. Page, L. Xue, S. Liu, J. Li, J. H. Edgar, A. Dréau, V. Jacques, P. Valvin, B. Gil, and G. Cassabois, Phys. Rev. Materials **3**, 094001 (2019).

[17] P. Valvin, T. Pelini, G. Cassabois, A. Zobelli, J. Li, J. H. Edgar, and B. Gil, AIP Adv. **10**, 075025 (2020).

[18] A. Rousseau, L. Ren, A. Durand, P. Valvin, B. Gil, K. Watanabe, T. Taniguchi, B. Urbaszek, X. Marie, C. Robert, and G. Cassabois, Nano Lett. **21**, 10133 (2021).

[19] T. Q. P. Vuong, S. Liu, A. Van der Lee, R. Cuscó, L. Artús, T. Michel, P. Valvin, J. H. Edgar, G. Cassabois, and B. Gil, Nat. Mater. **17**, 152 (2018).

[20] T. Q. P. Vuong, G. Cassabois, P. Valvin, V. Jacques, A. Van Der Lee, A. Zobelli, K. Watanabe, T. Taniguchi, and B. Gil, 2D Mater. **4**, 011004 (2017).

[21] R. Schuster, C. Habenicht, M. Ahmad, M. Knupfer, and B. Büchner, Phys. Rev. B **97**, 041201(R) (2018).

[22] T. Q. P. Vuong, G. Cassabois, P. Valvin, V. Jacques, R. Cuscó, L. Artús, and B. Gil, Phys. Rev. B **95**, 045207 (2017).

[23] P. Y. Yu and M. Cardona, *Fundamentals of Semiconductors* (Springer-Verlag, Berlin, 1996).

[24] C. F. Klingshirn, *Semiconductor Optics* (Springer-Verlag, Berlin, 2007).

[25] L. C. Andreani, in *Confined Electrons and Photons: New Physics and Applications*, edited by E. Burnstein and C. Weisbuch, NATO Science Series B (Plenum Press, New York, 1995), p. 57.

[26] T. Q. P. Vuong, G. Cassabois, P. Valvin, S. Liu, J. H. Edgar, and B. Gil, Phys. Rev. B **95**, 201202(R) (2017).

[27] S. Rudin, T. L. Reinecke, and B. Segall, Phys. Rev. B **42**, 11218 (1990).

[28] Y. Toyozawa, Prog. Theor. Phys. **20**, 53 (1958).

[29] G. Cassabois, A. L. C. Triques, F. Bogani, C. Delalande, Ph. Roussignol, and C. Piermarocchi, Phys. Rev. B **61**, 1696 (2000).